Surface Quasigeostrophic Solutions and Baroclinic Modes with Exponential Stratification

J. H. LACASCE

Department of Geosciences, University of Oslo, Oslo, Norway

(Manuscript received 22 June 2011, in final form 26 October 2011)

ABSTRACT

The author derives baroclinic modes and surface quasigeostrophic (SQG) solutions with exponential stratification and compares the results to those obtained with constant stratification. The SQG solutions with exponential stratification decay more rapidly in the vertical and have weaker near-surface velocities. This then compounds the previously noted problem that SQG underpredicts the velocities associated with a given surface density anomaly.

The author also examines how the SQG solutions project onto the baroclinic modes. With constant stratification, SQG waves larger than deformation scale project primarily onto the barotropic mode and to a lesser degree onto the first baroclinic mode. However, with exponential stratification, the largest projection is on the first baroclinic mode. The effect is even more pronounced over rough bottom topography. Therefore, large-scale SQG waves will look like the first baroclinic mode and vice versa, with realistic stratification.

1. Introduction

There has been substantial interest in recent years in the surface quasigeostrophic (SQG) approximation, as a simplified dynamical model for the atmosphere and ocean. The SQG solutions derive from the Eady (1949) model of baroclinic instability, representing temperature anomalies confined to a boundary with zero or constant potential vorticity (PV) in the interior of the fluid. In the Eady model, the anomalies lie on rigid upper and lower boundaries, and instability occurs when anomalies on one boundary couple with those on the other. Blumen (1978) studied the finite-amplitude properties of SQG waves. Fully turbulent flow exists in the SQG system and, as in conventional 2D turbulence, there are two inertial ranges. Total energy (kinetic plus potential) cascades to larger scales and temperature variance (the analog of enstrophy in SQG) cascades to small scales. These properties were explored further by Held et al. (1995).

In the atmosphere, SQG has been used to understand flow near the tropopause. In such studies, the tropopause is treated as a boundary and the tropospheric PV is assumed constant. Juckes (1994) demonstrated that such an idealization yielded a flow similar to that found in a general circulation model. Hakim et al. (2002) extended the analogy, showing that a modified version of SQG (which retains the next highest-order terms in the Rossby number expansion) can account for the observed asymmetry between cyclones and anticyclones near the tropopause. SQG has further been used to rationalize kinetic energy spectra in the troposphere (Tulloch and Smith 2006, 2009).

There has also been interest in applying SQG to the near-surface flow in the ocean. In this case, the flow is linked to anomalies in density at the surface. The idea was explored by Lapeyre and Klein (2006), using data from a model of the Antarctic Circumpolar Current (ACC), and by LaCasce and Mahadevan (2006), using in situ observations from the Mediterranean, eastern Pacific, and eastern Atlantic. In most cases, SQG yielded a plausible representation of the subsurface flow. Similar projections have been explored by Isern-Fontanet et al. (2008), Capet et al. (2008), Klein et al. (2008), and others.

In the preceding studies, the SQG formalism (described later) was applied assuming the Brunt–Väisälä frequency $N(z)$ was constant. This simplifies the calculations, because the solutions are exponentials (or hyperbolic sines and cosines; see section 2a). However, although a constant Brunt–Väisälä frequency is defensible in the troposphere,

Corresponding author address: Joe LaCasce, Department of Geosciences, University of Oslo, P.O. Box 1022 Blindern, N-0315 Oslo, Norway.
E-mail: j.h.lacasce@geo.uio.no

DOI: 10.1175/JPO-D-11-0111.1

it is not realistic in the ocean where the stratification is surface intensified. Using realistic stratification will presumably alter the vertical structure of the solutions.

Indeed, the vertical structure is a significant issue when applying SQG to the ocean; with a constant N, the predicted subsurface velocities decay too rapidly with depth. In an example from the western Mediterranean studied by LaCasce and Mahadevan (2006), the predicted velocities at 100-m depth, though qualitatively similar to the observed, were less than half as strong. Similar discrepancies were seen in other regions and also in models (Lapeyre and Klein 2006).

Various "fixes" have been proposed. Lapeyre and Klein (2006) suggested that N be treated as an adjustable parameter [the "effective SQG" (eSQG) method; Isern-Fontanet et al. 2008; Lapeyre 2009]. LaCasce and Mahadevan (2006) proposed instead including a subsurface PV, slaved to the surface density. Both methods possess a parameter that can be adjusted to increase the depth of penetration. However, it is possible that the SQG vertical structure is simply incorrect and that this stems from using constant stratification.

Current meter data, on the other hand, are often analyzed in terms of baroclinic modes. These are usually determined numerically, using observed profiles of $N(z)$. An early such calculation was made by Kundu et al. (1975), who solved the Sturm–Liouville problem numerically using stratification off the Oregon coast. In an extensive examination of current meter data from the Northern Hemisphere, Wunsch (1997) found that the fluctuating kinetic energy is dominated by the barotropic and first baroclinic modes, with the latter dominating near the surface. This implies that surface altimetry primarily reflects that mode.

But how does one reconcile this with SQG? Because the baroclinic modes form a complete set, the SQG solutions necessarily project onto them (e.g., Ferrari and Wunsch 2010). This is true even though the baroclinic modes have no density anomaly at the upper surface; with a large number of modes, the projection simply fails to capture the SQG response on the boundary itself [in line with the Bretherton (1966) notion of the surface density as a delta function of PV]. However, in order to consider the projection of the SQG solutions on the baroclinic modes, one must use the same stratification for both solutions.

Lapeyre (2009) has examined similar issues, but from a slightly different perspective. He considered the projection onto vertical modes as "incomplete" and added an explicit term representing the surface mode. He then examined cases with realistic stratification, solving the Sturm–Liouville problem numerically. In contrast, we recognize the baroclinic modes as a complete, orthogonal set and ask how a given SQG wave projects onto them. We focus on one density profile (exponential) and solve the problem analytically.

Thus, there are two goals for the present article. One is to answer the question about the vertical scale of SQG-like motion with more realistic stratification. The second is to see how SQG motion would appear in terms of baroclinic modes.

2. Theory

The SQG and baroclinic mode solutions derive from the linear quasigeostrophic potential vorticity (QGPV) equation,

$$\frac{\partial}{\partial t}\left[\nabla^2\psi + \frac{\partial}{\partial z}\left(\frac{f_0^2}{N^2}\frac{\partial}{\partial z}\psi\right)\right] + \beta\frac{\partial}{\partial x}\psi = 0, \tag{1}$$

where f_0 is the mean Coriolis parameter, $N(z)$ is the Brunt–Väisälä frequency, and $\psi = p/(f_0\rho_0)$ is the geostrophic streamfunction (if p is the pressure and ρ_0 is the average density; Pedlosky 1987). Assuming a solution that is wave-like in the horizontal,

$$\psi(x, y, z, t) = \phi(z)\hat{\psi}_{k,l,\omega}e^{ikx+ily-i\omega t}, \tag{2}$$

and substituting this into (1) yields an ODE for the vertical structure, $\phi(z)$,

$$\frac{d}{dz}\left(\frac{f_0^2}{N^2}\frac{d\phi}{dz}\right) + \lambda^2\phi = 0, \tag{3}$$

where $\lambda^2 = -[k^2 + l^2 + \beta/(k\omega)]$.

For the boundary conditions, one generally assumes flat surfaces where

$$\frac{d\phi}{dz} = 0, \quad z = 0, -H. \tag{4}$$

This implies that the perturbation density vanishes at the boundaries, which follows from the hydrostatic relation. Specifically,

$$\rho = -\frac{1}{g}\frac{\partial}{\partial z}p = -\frac{f_0\rho_0}{g}\frac{\partial}{\partial z}\psi = -\frac{f_0\rho_0}{g}\frac{d\phi}{dz}\hat{\psi}_{k,l,\omega}e^{ikx+ily-i\omega t}. \tag{5}$$

The resulting Sturm–Liouville problem [(3) and (4)] yields a complete set of orthogonal eigenmodes (e.g., Gill 1982; Kundu et al. 1975; Philander 1978; Pedlosky 1987; Wunsch and Stammer 1997) given that λ^2 is positive. The zeroth eigenmode is the barotropic mode, and

the higher-order modes are the baroclinic modes. We refer to $\phi(z)$ here as the interior portion of the solution.

The SQG solutions on the other hand are linked to buoyancy anomalies on the bounding surfaces, assuming constant PV in the fluid interior. The constant is usually taken to be zero. Again, assuming a wave dependence in (x, y, t),

$$\psi(x, y, z, t) = \chi(z)\hat{\psi}_{k,l,\omega}e^{ikx+ily-i\omega t}, \tag{6}$$

having zero PV implies

$$\frac{d}{dz}\left(\frac{f_0^2}{N^2}\frac{d\chi}{dz}\right) - \kappa^2\chi = 0, \tag{7}$$

where $\kappa = (k^2 + l^2)^{1/2}$ is the magnitude of the horizontal wavenumber. Note that (7) is the same as (3) on the f plane; with $\beta = 0$, there is no interior PV gradient and λ^2 is negative. As such, the SQG solutions resemble the ''negative depth modes'' of Longuet-Higgins (1968) and Philander (1978). The boundary conditions are slightly different though. Replacing ϕ with χ in the hydrostatic relation (5), we require

$$\frac{d\chi}{dz}(0) = 1, \quad \frac{d\chi}{dz}(-H) = 0. \tag{8}$$

Thus, the SQG solutions have a nonvanishing surface buoyancy on the upper (surface) boundary.

In the SQG framework, the streamfunction ψ is determined by the surface density,

$$\hat{\psi}_{k,l,\omega} = -\frac{g}{f_0\rho_0}\hat{\rho}_{k,l,\omega}. \tag{9}$$

Thus, the flow field can be reconstructed from the surface density alone. Note too that, in contrast to the discrete baroclinic modes, there is a continuum of SQG solutions (assuming a continuous set of horizontal wavenumbers).

a. Constant N

The interior solutions to (3) and (4) with N = constant are well known (Pedlosky 1987),

$$\phi = A\cos\left(\frac{n\pi z}{H}\right), \tag{10}$$

where n is an integer. The barotropic mode ($n = 0$) is depth invariant and the first baroclinic mode ($n = 1$) has a single zero crossing. Further, the amplitude at the surface is equal in magnitude to that at the bottom.

The SQG solution to (7) with constant stratification and which satisfies the lower boundary condition in (8) is

$$\chi = A_0\cosh\left[\frac{\kappa N}{f_0}(z + H)\right] \tag{11}$$

(Tulloch and Smith 2006). The constant A_0 is determined by the surface condition in (8). The result is

$$\chi = \frac{H\kappa_d}{\kappa}\frac{\cosh[(1 + z/H)\kappa/\kappa_d]}{\sinh(\kappa/\kappa_d)}, \tag{12}$$

where $\kappa_d \equiv f_0/(NH)$ is inversely proportional to the deformation radius. Instead of being sinusoidal, like the interior modes, the SQG solutions are exponential in character. Indeed, in the limit of strong stratification (large N), the solutions decay exponentially with depth.

As noted, the SQG solutions project onto the interior modes, because the latter form a complete basis. So we can write

$$\chi(z) = \sum_{n=0}^{N} C_n\cos\left(\frac{n\pi z}{H}\right). \tag{13}$$

The coefficients C_n are then given by

$$C_n = \frac{2}{H}\int_{-H}^{0}\chi\cos\left(\frac{n\pi z}{H}\right)dz = \frac{2H}{n^2\pi^2 + \kappa^2/\kappa_d^2}, \quad n \geq 1 \tag{14}$$

and

$$C_0 = \frac{H\kappa_d^2}{\kappa^2} \tag{15}$$

for $n = 0$. The projection depends strongly on the wavelength of the SQG wave, because the SQG wave's horizontal scale determines its vertical scale. The modes that contribute the most are those for which $n^2\pi^2 < \kappa^2/\kappa_d^2$. The larger that κ/κ_d is, the more baroclinic modes that are required. Waves much larger than κ_d^{-1} project primarily onto the gravest modes, whereas smaller waves project onto higher modes.

b. Exponential N

For our surface-intensified stratification, we use an exponential profile,

$$N^2 = N_0^2e^{\alpha z}. \tag{16}$$

Vertical modes with exponential stratification have been discussed previously in the context of internal waves (e.g., Krauss 1966; Garrett and Munk 1972; Philander 1978). Substituting (16) into (3) yields

$$\frac{d^2\phi}{dz^2} - \alpha\frac{d\phi}{dz} + \frac{N_0^2\lambda^2}{f_0^2}e^{\alpha z}\phi = 0. \quad (17)$$

With the substitution $\zeta = e^{\alpha z/2}$, we recover a Bessel-type equation,

$$\zeta^2\frac{d^2\phi}{d\zeta^2} - \zeta\frac{d\phi}{d\zeta} + \frac{4N_0^2\lambda^2}{\alpha^2 f_0^2}\zeta^2\phi = 0. \quad (18)$$

The solution that satisfies the upper boundary condition in (4) (and written in terms of z) is

$$\phi = Ae^{\alpha z/2}[Y_0(2\gamma)J_1(2\gamma e^{\alpha z/2}) - J_0(2\gamma)Y_1(2\gamma e^{\alpha z/2})], \quad (19)$$

where $\gamma = N_0\lambda/(\alpha f_0)$. Imposing the bottom boundary condition yields

$$J_0(2\gamma)Y_0(2\gamma e^{-\alpha H/2}) - Y_0(2\gamma)J_0(2\gamma e^{-\alpha H/2}) = 0. \quad (20)$$

This transcendental equation is satisfied for discrete eigenvalues of γ. We solve this numerically later, using the Newton–Raphson algorithm.

The SQG equation can be obtained by substituting $i\kappa$ for λ in the modal Eq. (17). The result is another Bessel equation, like (18). However, because the last term has changed signs, the solution involves modified Bessel functions,

$$\chi = Ae^{\alpha z/2}I_1(2\eta e^{\alpha z/2}) + Be^{\alpha z/2}K_1(2\eta e^{\alpha z/2}), \quad (21)$$

where $\eta = N_0\kappa/(\alpha f_0) = (\kappa/\kappa_d)(\alpha H)^{-1}$. Imposing the surface and bottom boundary conditions yields

$$\chi = \frac{e^{\alpha z/2}}{\eta\alpha} \times \frac{K_0(2\eta e^{-\alpha H/2})I_1(2\eta e^{\alpha z/2}) + I_0(2\eta e^{-\alpha H/2})K_1(2\eta e^{\alpha z/2})}{I_0(2\eta)K_0(2\eta e^{-\alpha H/2}) - I_0(2\eta e^{-\alpha H/2})K_0(2\eta)}. \quad (22)$$

Equation (22) can be compared to the result with constant stratification given in (12). In the latter, the vertical scale is determined solely by the ratio κ/κ_d: that is, the ratio of the scale of motion to the deformation radius. However, in the exponential case in (22), the solution also depends on the e-folding scale of the stratification α^{-1}. As such, the vertical scale of the solution also depends on that of the stratification. This effect is entirely absent with constant stratification.

We can project the SQG solution onto the interior modes by solving

$$C_n = \frac{1}{\mathcal{D}}\int_{-H}^{0}\chi e^{\alpha z/2}[Y_0(2\gamma)J_1(2\gamma e^{\alpha z/2}) - J_0(2\gamma)Y_1(2\gamma e^{\alpha z/2})]\,dz, \quad (23)$$

where $\mathcal{D}$ is a normalization constant. As with the transcendental equation for γ, we will solve this numerically.

Another case with surface-intensified stratification that can be solved analytically was proposed by Lindzen (1994). This has

$$N^2 = \frac{N_0^2}{1 - Dz}. \quad (24)$$

The solutions are similar to those with exponential stratification (see appendix), particularly when the e-folding scale α^{-1} is large. Given this, we will focus solely on the exponential profile hereafter.

3. Results

a. Vertical modes

The baroclinic modes obtained with constant and exponential stratification are shown in Fig. 1. The cosine modes with constant stratification (Fig. 1, top left) are familiar, with equal amplitudes at the surface and bottom. For the exponential case, we must first solve Eq. (20) for the eigenvalues, and these depend on the vertical decay rate, α. We will examine two values, $\alpha = 2/H$ and $\alpha = 10/H$. These yield a ''thermocline'' in the upper half and tenth of the water column, respectively. The first four eigenvalues for both cases are given in Table 1.

The baroclinic modes with $\alpha = 2/H$ are plotted in Fig. 1 (top right). These resemble the constant N modes in that the number of zero crossings increases with mode number. However, the amplitudes are greatest at the surface, and the vertical wavelength increases with depth. These tendencies are more pronounced with $\alpha = 10/H$ (Fig. 1, bottom left), with the zero crossings confined to the thermocline region in the upper 10% of the water column. Below that, the modes have little shear.

The latter exponential modes resemble those seen in many observations: for example, the observations of Kundu et al. (1975). In their case, the stratification decays with depth, with the strongest gradients in the upper fifth of the water column. Their modes likewise exhibit the greatest variability near the surface (their Fig. 7), where the stratification is strongest. The primary difference is that they also had a surface mixed layer, with the result that their modes had little shear near the

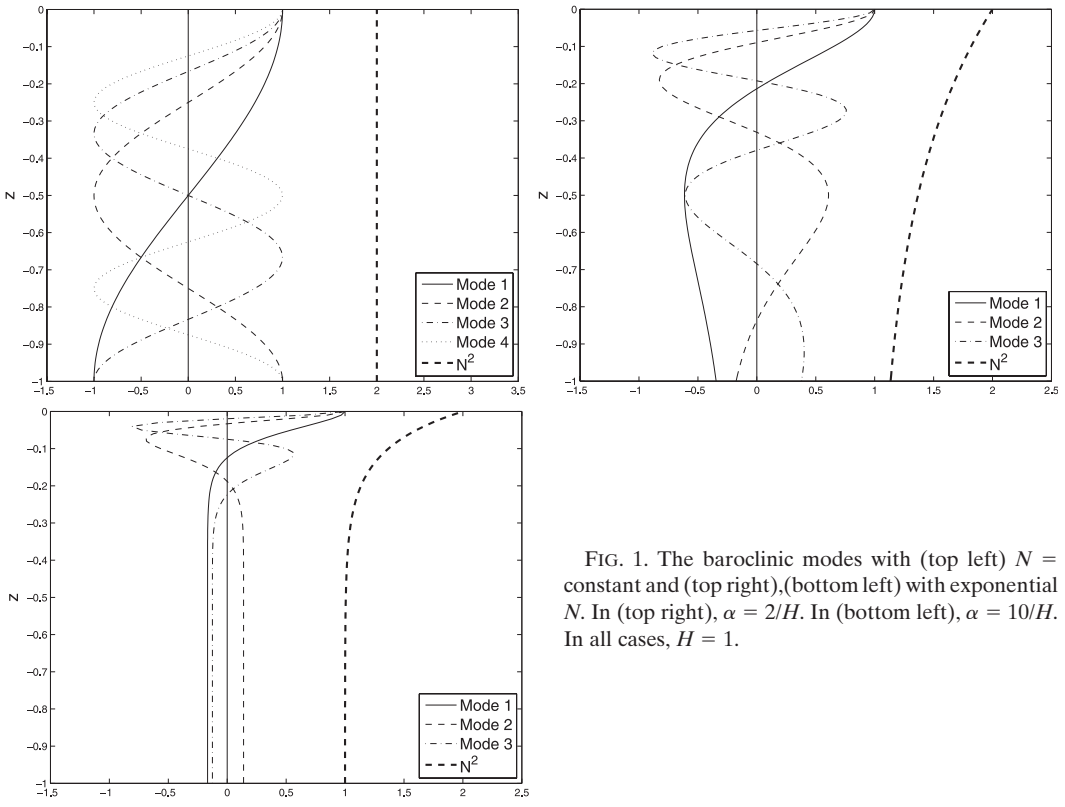

FIG. 1. The baroclinic modes with (top left) N = constant and (top right),(bottom left) with exponential N. In (top right), $\alpha = 2/H$. In (bottom left), $\alpha = 10/H$. In all cases, $H = 1$.

surface itself. Comparing with the exponential modes, it appears the mixed layer alters the modal structure in the mixed layer itself; below that, the structure is very similar.

b. SQG solutions

Now we compare the constant and exponential stratification solutions to (7). To do this, we take the constant Brunt–Väisälä frequency to be equal to the exponential N at the surface (as was done, e.g., by LaCasce and Mahadevan 2006). We must also choose the horizontal scale of the SQG wave, which in turn determines its vertical scale. A useful reference is the deformation radius, the scale of the first baroclinic mode. With constant stratification, the first mode has a wavenumber of $\lambda_1 = \pi f_0/(NH) = \pi\kappa_d$ (Table 1). So a deformation scale SQG wave has $\kappa = \pi\kappa_d$. With exponential stratification, the first mode has a wavenumber of $\lambda_1 = \alpha f_0 x_1/(2N_0)$, where $x_1 = 2\gamma_1$ is the first eigenvalue from Eq. (20). Thus, a deformation scale SQG wave has $\eta = N_0\lambda_1/(\alpha f_0) = x_1/2$.

In Fig. 2, we plot $d\chi/dz$ against depth for two different e-folding depths and two horizontal wavenumbers ($2\lambda_1$ and $0.5\lambda_1$). Recall that $d\chi/dz$ reflects the density and that $d\chi/dz = 1$ at the surface in all cases. With the deeper e-folding scale ($\alpha = 2/H$; Fig. 2, top), the profiles are similar, particularly for the smaller SQG wave ($\kappa = 2\lambda_1$; Fig. 2, top right). However, the density for the exponential stratification decays more rapidly with depth, in both cases. The differences are more pronounced though with the shallow e-folding depth ($\alpha = 10/H$; Fig. 2, bottom). In both cases, the signal decays much more rapidly in the vertical for the exponential solutions.

In Fig. 3, we plot χ, which reflects the streamfunction (and hence the horizontal velocities). Again, the structure is similar for the two cases when the SQG wave is subdeformation scale and when the e-folding depth is large ($\alpha = 2/H$; Fig. 3, top right). However, even in this case, the surface streamfunction is less with exponential stratification. This implies the surface velocities are weaker than with constant stratification, given the same

TABLE 1. The first five eigenvalues for the baroclinic modes with different stratification. The values for the exponential and Lindzen profiles are for 2γ, as in Eqs. (20) and (A4), respectively.

Mode	Constant N	Exponential ($\alpha = 2/H$)	Exponential ($\alpha = 10/H$)	Lindzen ($D = 10/H$)
1	π	4.9107	2.7565	1.4214
2	2π	9.9072	5.9590	2.7506
3	3π	14.8875	9.1492	4.0950
4	4π	19.8628	12.334	5.4448

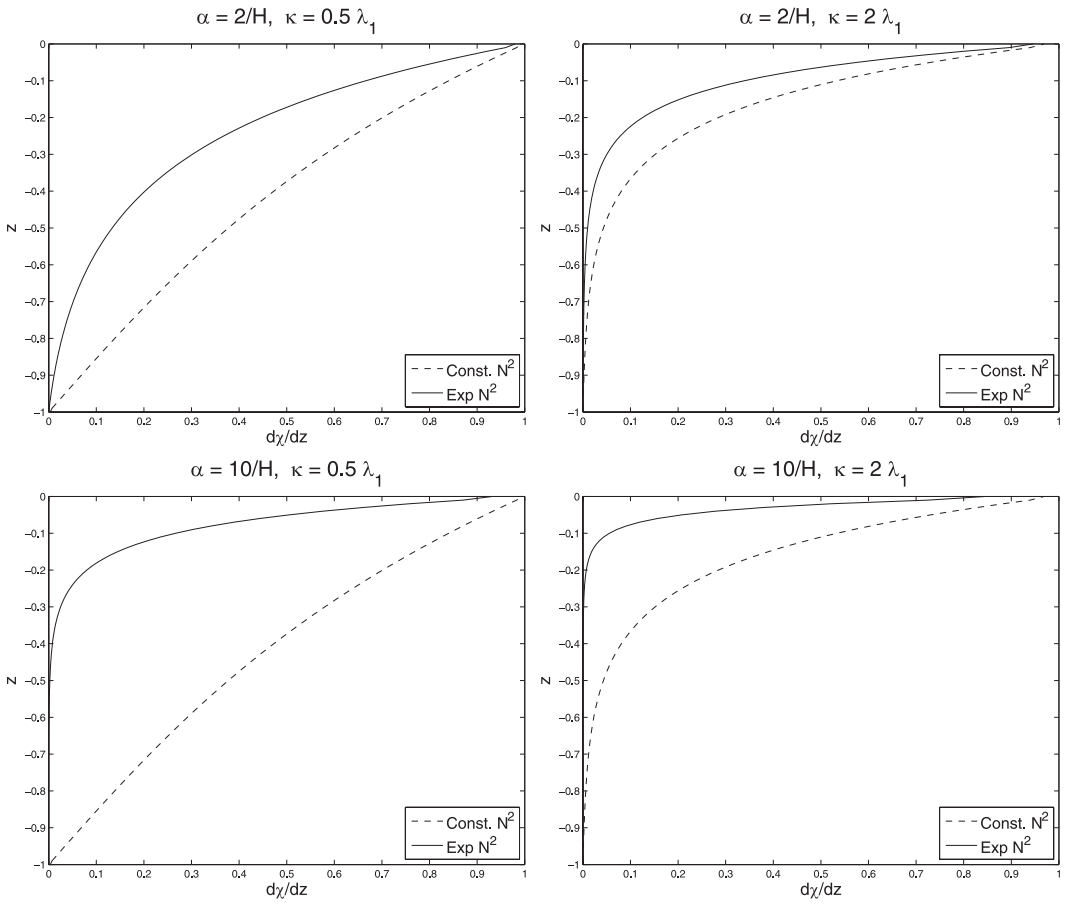

FIG. 2. The vertical derivatives of the SQG vertical structure $\chi(z)$, with constant (solid curves) and exponential N (dashed) for waves (left) twice and (right) half the deformation scale: (top) $\alpha = 2/H$ and (bottom) $\alpha = 10/H$.

surface density anomaly. The difference is greater for the larger wave (Fig. 3, top left), and greater still for the shallow e-folding depth $\alpha = 10/H$ (Fig. 3, bottom). For the case with $\kappa = 0.5\kappa_d$ (Fig. 3, bottom left), the streamfunction amplitude is roughly 7 times less than with constant stratification.

Having exponential stratification thus has two effects on the SQG solutions. First, the vertical decay is more rapid than with constant stratification. This is because the stratification itself limits the vertical penetration of the SQG wave. This can be seen in solution (22), which has a prefactor of $\exp(\alpha z/2)$. No such modification occurs with constant stratification, where the vertical scale is determined solely by the horizontal scale of the wave. Waves larger than deformation scale easily reach the bottom.

Second, the velocities associated with surface density anomalies are weaker with exponential stratification. This follows from the surface boundary condition, which demands that $d\phi/dz = 1$. Scaling this, we infer that $\phi(0) \propto D$, if D is the vertical scale of the motion. Because the horizontal velocities are proportional to ϕ, they likewise scale with the vertical height. With exponential stratification, D is much less than with constant stratification, so the velocities associated with a given density anomaly are weaker.

c. *Projections onto vertical modes*

The other question is how SQG-like motion would appear in terms of the interior modes. Consider the case with constant stratification first. Two projections, for SQG waves with $\kappa = 0.5\lambda_1$ and $\kappa = 2\lambda_1$, are shown in Fig. 4. The SQG wave vertical structure $\chi(z)$ is indicated by the curve with squares, and the projections onto the barotropic and first three baroclinic modes are also shown.

The larger SQG wave (Fig. 4, left) decays slowly with depth and thus has a large depth-averaged component. Accordingly, 85% of the variance is in the barotropic mode. A further 14% is in the first baroclinic mode, so these two account for 99% of the variance. This is perhaps unsurprising, because the SQG wave has no zero crossing and a nonzero depth average.

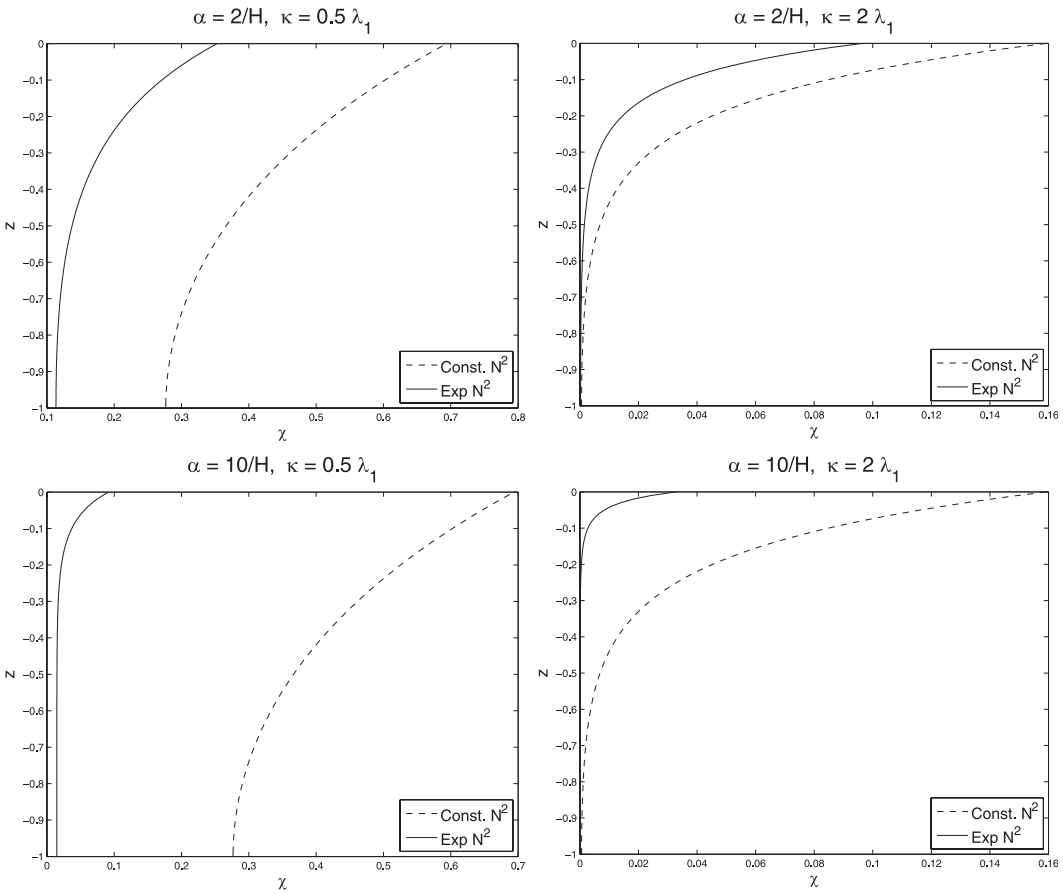

FIG. 3. The SQG vertical structure $\chi(z)$, with constant and exponential N. The format is as in Fig. 2.

The smaller wave (Fig. 4, right) decays more rapidly with depth, and its depth average is less. Only 19% of the variance is in the barotropic mode, and 49% is in the first baroclinic mode. The higher modes accordingly account for the remaining 32%.

The results with exponential stratification, with a deep e-folding scale ($\alpha = 2/H$), are shown in Fig. 5. As with constant stratification, the SQG wave with $\kappa = 0.5\lambda_1$ (Fig. 5, left) decays slowly with depth and has a significant depth average. As such, the barotropic projection accounts for 67% of the variance. The first baroclinic mode has 28% of the variance, so again the first two modes account for 95%. The subdeformation scale wave (Fig. 5, right) decays more rapidly and projects onto a wider range of vertical modes. The barotropic mode accounts for only 8% of the variance, whereas the first baroclinic mode captures 50%. The higher modes account for the remaining 42%.

The picture changes though with a shallower thermocline, as the SQG wave decays more rapidly with depth. The wave with $\kappa = 0.5\lambda_1$ (Fig. 6, left) decays significantly in the upper fifth of the water column and has a relatively weak (15%) projection onto the barotropic mode. Rather, the wave projects primarily onto the first baroclinic mode (69%). Indeed, the SQG wave with this stratification resembles the first baroclinic mode, except that the latter has a zero crossing. Again, the higher modes account for less of the variance (15%). As in the previous cases, more baroclinic modes are required to capture the smaller wave ($\kappa = 2\lambda_1$; Fig. 6, right). Nevertheless, the largest fraction of the variance (38%) is in the first baroclinic mode, which has a structure closest to the SQG wave.

d. Projection with rough topography

SQG waves with exponential stratification and a shallow thermocline resemble the first baroclinic mode, except that the latter has a zero crossing and oppositely directed flow at depth. This begs the question of what the projection would look like if there were no flow at the bottom: that is, if the bottom boundary condition were $u = v = 0$ rather than $w = 0$. This is the case if the bottom slope is steep (such that the depth changes appreciably over the length scale of the motion; Pedlosky 1987). The

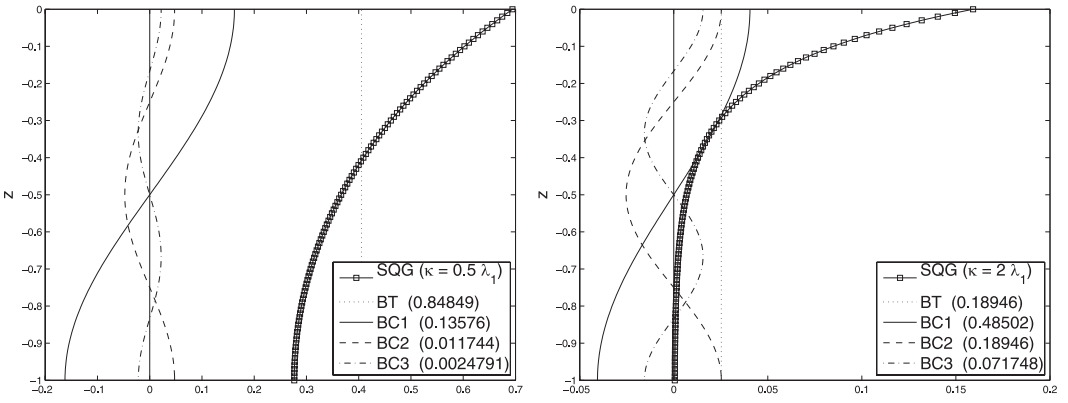

FIG. 4. The projection of the SQG solution with constant stratification onto vertical modes. The SQG vertical structure χ is indicated by the curve with squares, for a wave with (left) $\kappa = 0.5\lambda_1$ and (right) $\kappa = 2\lambda_1$. The barotropic projection is indicated by the vertical dotted line, and the projection onto the first baroclinic mode is indicated by the solid curve. The projections onto the next two baroclinic modes are also plotted. Indicated in the boxes in the bottom right is the fraction of the variance in each mode.

same condition was used by Samelson (1992) in his study of the surface intensification of Rossby waves. With no horizontal flow at the bottom, the barotropic mode vanishes (it is replaced by a bottom-intensified topographic wave mode) and all the baroclinic modes have a node at the bottom. Thus, the first baroclinic mode has no zero crossing in the interior of the fluid.

To examine this, we rederived the exponential solutions, changing the bottom boundary condition to $\phi(-H) = 0$ [for Eq. (17)] and $\chi(-H) = 0$. The baroclinic modes have the same form as in (19), but the transcendental Eq. (20) changes to

$$J_0(2\gamma)Y_1(2\gamma e^{-\alpha H/2}) - Y_0(2\gamma)J_1(2\gamma e^{-\alpha H/2}) = 0. \tag{25}$$

Likewise, the SQG solution (22) changes slightly, to

$$\chi = \frac{e^{\alpha z/2}}{\eta\alpha}\frac{K_1(2\eta e^{-\alpha H/2})I_1(2\eta e^{\alpha z/2}) - I_1(2\eta e^{-\alpha H/2})K_1(2\eta e^{\alpha z/2})}{I_1(2\eta)K_0(2\eta e^{-\alpha H/2}) + I_0(2\eta e^{-\alpha H/2})K_1(2\eta)}. \tag{26}$$

As before, we solve the transcendental equation and project the SQG waves onto the vertical modes numerically.

The projections are shown in Fig. 7, for the case with $\alpha = 10/H$. Now the larger SQG wave ($\kappa = 0.5\lambda_1$; Fig. 7, left) projects almost entirely onto the first baroclinic mode (86%). Both are surface intensified and decay to zero at depth. Nevertheless, the higher modes are present, because the SQG wave decays more rapidly with depth than the first baroclinic mode. The smaller

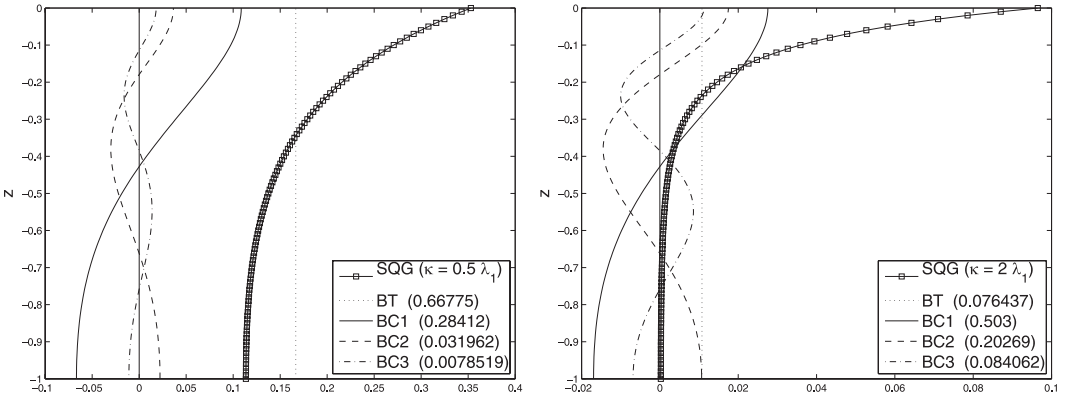

FIG. 5. The SQG projections with exponential stratification with $\alpha = 2/H$. The format is as in Fig. 4.

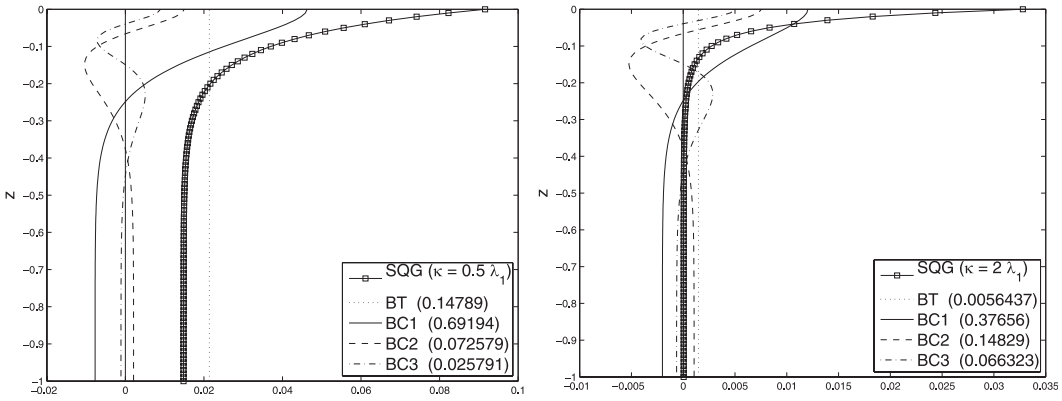

FIG. 6. The SQG projections with exponential stratification with $\alpha = 10/H$.

SQG wave (Fig. 7, right) also has a large projection onto the first baroclinic mode (45%). This is greater than in any of the previous examples with ($\kappa = 2\lambda_1$). Thus, with zero flow at the bottom, the SQG waves closely resemble the first baroclinic mode.

e. Effect on spectra

Finally, we consider how variable stratification affects the kinetic energy and buoyancy spectra. As pointed out by Isern-Fontanet et al. (2008), these are proportional under surface quasi geostrophy with constant stratification. Thus, if KE $\propto \kappa^{-5/3}$, the buoyancy has the same slope.

Consider the flow at the surface. From (5) we have

$$B = \frac{1}{2}|\hat{\rho}|^2 = \frac{1}{2}\left(\frac{f_0\rho_0}{g}\right)^2\left(\frac{d\chi}{dz}\right)^2|\hat{\psi}|^2 = \frac{1}{2}\left(\frac{f_0\rho_0}{g}\right)^2|\hat{\psi}|^2 \quad (27)$$

and

$$\mathrm{KE} = \frac{1}{2}\left(|\hat{u}|^2 + |\hat{v}|^2\right) = \frac{1}{2}\left(\frac{f_0\rho_0}{g}\right)^2\chi(0)^2\kappa^2|\hat{\psi}|^2 \quad (28)$$

Using the SQG solution with constant stratification (12), we have

$$\mathrm{KE} = \frac{1}{2}\left(\frac{f_0\rho_0 H}{g\kappa_d}\right)^2\coth^2\left(\frac{\kappa}{\kappa_d}\right)|\hat{\psi}|^2. \quad (29)$$

The dependence of KE on wavenumber is shown in Fig. 8. Here, we plot $\chi^2(z = 0)$ normalized by the value at $\kappa = \kappa_d$. At small scales ($\kappa > \kappa_d$), $\chi^2(0)$ asymptotes to one, implying the kinetic energy spectrum is proportional to the buoyancy spectrum. At wavenumbers smaller than κ_d though, $\coth^2(\kappa/\kappa_d)$ is proportional to κ^{-2}, so the kinetic energy spectrum is steeper than the buoyancy spectrum. This is a finite depth effect, because only the large-scale waves penetrate deep enough to feel the bottom.

With exponential stratification, the buoyancy spectrum at the surface has the same form as above (because the boundary condition is the same). However, the kinetic energy spectrum (28) now depends on the square of the SQG solution (22). This is indicated by the dashed curve in Fig. 8, for the case $\alpha = 10/H$. At large scales, the curve is proportional to κ^{-4}, implying the kinetic energy spectrum

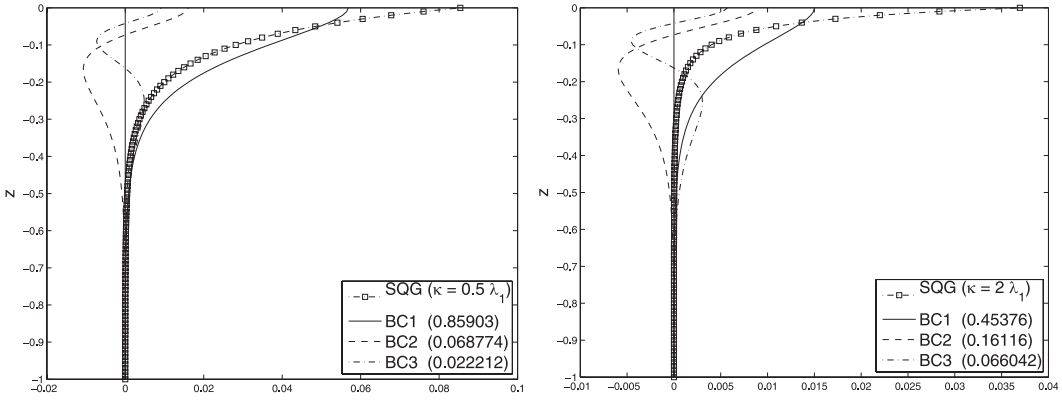

FIG. 7. The SQG projections with exponential stratification with $\alpha = 10/H$ and assuming rough bottom topography (zero flow at $z = -H$).

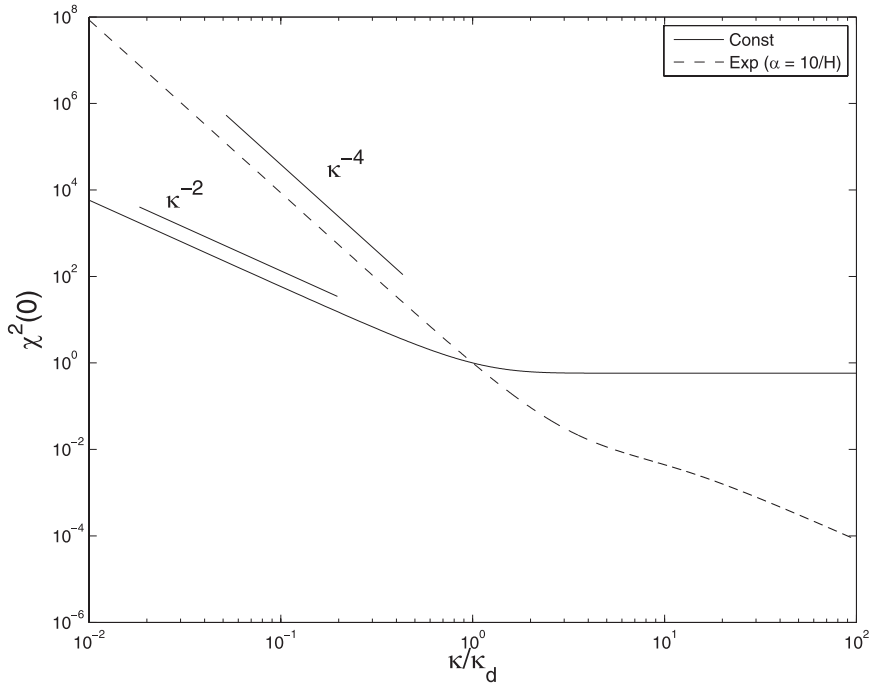

FIG. 8. The ratio between the kinetic energy and buoyancy spectra as a function of wavenumber. Shown is the quantity $\chi^2(0)$, plotted against κ/κ_d and normalized by the value at $\kappa = \kappa_d$. The solution with constant stratification is shown by the solid curve and the exponential solution, with $\alpha = 10/H$, is shown by the dashed curve.

is much steeper. However, even with $\kappa > \kappa_d$, the curve is not flat, implying the KE spectrum is steeper. Thus, the energy spectrum differs from the buoyancy spectrum at all scales with exponential stratification. So the spectra are not expected to be similar under realistic conditions.

4. Summary and discussion

We have compared surface quasigeostrophic (SQG) solutions with exponential stratification to those obtained with constant stratification (as is often used in SQG studies). Assuming the same Brunt–Väisälä frequency at the surface, the solutions with exponential stratification decay more rapidly with depth, because the solutions depend on the stratification itself. This effect is absent with constant stratification, where the vertical scale depends only on the horizontal scale of the wave and N_0. In addition, the SQG streamfunction is weaker with exponential stratification. This implies that, for the same surface density gradient, the horizontal velocities are weaker with exponential stratification. With the thermocline in the upper 10% of the water column, the velocities for a wave twice the size of the first deformation radius are 7 times weaker than those obtained with constant stratification.

We also examined how SQG waves project onto traditional baroclinic modes. With constant stratification, waves larger than deformation scale project primarily onto the barotropic mode and, to a lesser extent, the first baroclinic mode. Smaller waves project more onto the higher baroclinic modes. With exponential stratification, the projection depends on the depth of the thermocline. With a deep thermocline, the results are similar to those with constant stratification because the stratification plays a lesser role in determining the vertical scale of the wave. However, with a shallow thermocline, the large SQG waves project more onto the first baroclinic mode, which has a similar structure. For solutions with rough bottom topography (no horizontal flow at the bottom), the SQG wave closely resembles the first baroclinic mode and projects largely onto it.

In addition, variable stratification affects the relation between the buoyancy and kinetic energy spectra. At subdeformation scales, the two spectra are proportional with constant stratification, as noted by Isern-Fontanet et al. (2008). However, with exponential stratification, the kinetic energy spectrum is steeper, at all scales.

As noted, previous studies suggest that SQG (with constant stratification) captures qualitatively the vertical structure of the flow but also underpredicts the amplitude of the subsurface velocities (LaCasce and Mahadevan 2006; Lapeyre and Klein 2006). The present results suggest that using realistic, surface-intensified

stratification will make matters worse, weakening not only the subsurface velocities but also those at the surface. One option is to treat N_0 as an adjustable parameter (Lapeyre and Klein 2006), but even larger values will now be required. Moreover, it is doubtful that a single correction will suffice, because different size waves have different vertical scales.

But why then does SQG capture the qualitative structure of the near-surface flow? The answer may be because the SQG solution with realistic stratification closely resembles the first baroclinic mode, particularly for large waves. Le Traon et al. (2008) suggest that SQG dynamics is applicable over the range of scales from tens of meters up to several hundred kilometers.[1] Because the energy spectra are red, this implies a large contribution from SQG waves larger than the deformation radius. Such waves would have a vertical structure like the first baroclinic mode. The similarity is even more striking if there is no horizontal flow at the bottom. Thus, if the near-surface dynamics are instead dominated by the first baroclinic mode, as suggested, for example, by Wunsch (1997), the flow will resemble that predicted by SQG. Therefore, SQG could yield a plausible representation of the subsurface flow simply because it resembles the first baroclinic mode.

Can SQG motion then be distinguished from more traditional QG motion? The present solutions suggest SQG waves decay slightly more rapidly than the first baroclinic mode. This suggests a way that SQG-like motion could be sought in the ocean. If, for example, the dominant EOF at a given location resembles the first baroclinic mode but also decays more rapidly with depth, then this could be an indication of SQG. If this is not the case (i.e., if the first EOF resembles the first baroclinic mode), then it would be sensible to assume surface height reflects the first baroclinic mode.

The subdeformation scales, on the other hand, remain an open question, because the motion is not well captured by the first baroclinic mode. However, it is not well captured by SQG either, which underpredicts the response with strong stratification. It remains to be seen whether a simplified representation of those scales exists.

Nevertheless, the fact that SQG, when adjusted to strengthen the subsurface response, correctly predicts the flow in some locations is suggestive. However, the assumption of zero PV in the interior is likely too strong. If there is subsurface PV and this is correlated with the surface density, the downward penetration could be much greater (LaCasce and Mahadevan 2006). Indeed, the surface expression may simply be part of a more complex picture. Future studies using, for example, high-resolution models with realistic basins, could shed light on this.

Acknowledgments. I have had many useful discussions with Amala Mahadevan, Rob Scott, Amit Tandon, and Carl Wunsch (who pointed out to me the similarity between the SQG solutions and negative depth modes). Two anonymous reviewers made a number of useful comments on the first draft and Jordi Isern-Fontanet suggested I discuss the effect on the spectra. The work was done in collaboration with NASA Project NNX10AE93G.

APPENDIX

Lindzen's Stratification

An alternate possibility for nonconstant stratification was proposed by Lindzen (1994) in a modified version of the Eady model (see also Isachsen 2011). In this, the Brunt–Väisälä frequency is given by

$$N^2 = \frac{N_0^2}{1 - Dz}. \tag{A1}$$

The stratification is surface intensified, as with the exponential profile. Indeed, if $|Dz| \ll 1$ and if $|\alpha z| \ll 1$ [in (16)], the two profiles are asymptotically the same if $\alpha = D$. Substituting (A1) into (3) yields

$$\frac{d^2}{dz^2}\phi - \frac{D}{1 - Dz}\frac{d}{dz}\phi + \frac{N_0^2\lambda^2}{f_0^2(1 - Dz)}\phi = 0 \tag{A2}$$

The solution that satisfies the upper boundary condition is

$$\phi = A[Y_1(2\gamma)J_0(2\gamma\sqrt{1 - Dz}) - J_1(2\gamma)Y_0(2\gamma\sqrt{1 - Dz})], \tag{A3}$$

where $\gamma \equiv N_0\lambda/(Df_0)$ and A is a constant. Applying the lower boundary condition yields a transcendental equation for γ,

$$Y_1(2\gamma)J_1(2\gamma\sqrt{1 + DH}) - J_1(2\gamma)Y_1(2\gamma\sqrt{1 + DH}) = 0. \tag{A4}$$

Eigenvalues with $D = 10/H$ are given in Table 1.

The SQG solution [to Eq. (7)] can be obtained by substituting $i\kappa$ for λ in (A2). Applying the boundary conditions yields

[1] Other studies differ on this view. The kinetic energy spectra of Wang et al. (2010) are steeper than expected for SQG and are more in line with traditional QG turbulence (Charney 1971).

$$\chi = \frac{1}{D\eta}\left[\frac{I_0(2\eta\sqrt{1-Dz})K_1(2\eta\sqrt{1+DH}) - K_0(2\eta\sqrt{1-Dz})I_1(2\eta\sqrt{1+DH})}{K_1(2\eta)I_1(2\eta\sqrt{1+DH}) - I_1(\eta)K_1(\eta\sqrt{1+DH})}\right], \quad \text{(A5)}$$

where $\eta = N_0\kappa/(Df_0)$. As with the exponential profile, the vertical decay of the stratification is reflected in the vertical scale of the SQG solution.

These solutions are quite similar to those with exponential stratification. Plotting the solutions, as well as the projections of the SQG solution onto the interior modes, yields results very like those with exponential stratification when the e-folding scale α^{-1} is large. As such, Lindzen's stratification yields results which are only modestly different than those obtained with constant stratification.

REFERENCES

Blumen, W., 1978: Uniform potential vorticity flow. Part I: Theory of wave interactions and two-dimensional turbulence. *J. Atmos. Sci.,* **35,** 774–783.

Bretherton, F. P., 1966: Critical layer instability in baroclinic flows. *Quart. J. Roy. Meteor. Soc.,* **92,** 325–334, doi:10.1002/qj.49709239302.

Capet, X., P. Klein, B. Hua, G. Lapeyre, and J. C. McWilliams, 2008: Surface kinetic energy transfer in surface quasi-geostrophic flows. *J. Fluid Mech.,* **604,** 165–174.

Charney, J., 1971: Geostrophic turbulence. *J. Atmos. Sci.,* **28,** 1087–1094.

Eady, E. T., 1949: Long waves and cyclone waves. *Tellus,* **1,** 33–52.

Ferrari, R., and C. Wunsch, 2010: The distribution of eddy kinetic and potential energies in the global ocean. *Tellus,* **62A,** 92–108.

Garrett, C., and W. Munk, 1972: Space-time scales of internal waves. *Geophys. Astrophys. Fluid Dyn.,* **3,** 225–264.

Gill, A., 1982: *Atmosphere–Ocean Dynamics*. Academic Press, 662 pp.

Hakim, G. J., C. Snyder, and D. J. Muraki, 2002: A new surface model for cyclone–anticyclone asymmetry. *J. Atmos. Sci.,* **59,** 2405–2420.

Held, I., R. Pierrehumbert, S. Garner, and K. Swanson, 1995: Surface quasi-geostrophic dynamics. *J. Fluid Mech.,* **282,** 1–20.

Isachsen, P. E., 2011: Baroclinic instability and eddy tracer transport across sloping bottom topography: How well does a modified Eady model do in primitive equation simulations? *Ocean Modell.,* **39,** 183–199, doi:10.1016/j.ocemod.2010.09.007.

Isern-Fontanet, J., B. Chapron, G. Lapeyre, and P. Klein, 2008: Potential use of microwave sea surface temperatures for the estimation of ocean currents. *Geophys. Res. Lett.,* **33,** L24608, doi:10.1029/2006GL027801.

Juckes, M., 1994: Quasigeostrophic dynamics of the tropopause. *J. Atmos. Sci.,* **51,** 2756–2768.

Klein, P., B. L. Hua, G. Lapeyre, X. Capet, S. L. Gentil, and H. Sasaki, 2008: Upper ocean turbulence from high-resolution 3D simulations. *J. Phys. Oceanogr.,* **38,** 1748–1763.

Krauss, W., 1966: *Interne Wellen*. Gebrder Borntraeger, 248 pp.

Kundu, P. K., J. S. Allen, and R. L. Smith, 1975: Modal decomposition of the velocity field near the Oregon coast. *J. Phys. Oceanogr.,* **5,** 683–704.

LaCasce, J., and A. Mahadevan, 2006: Estimating subsurface horizontal and vertical velocities from sea surface temperature. *J. Mar. Res.,* **64,** 695–721.

Lapeyre, G., 2009: What vertical mode does the altimeter reflect? On the decomposition in baroclinic modes on a surface-trapped mode. *J. Phys. Oceanogr.,* **39,** 2857–2874.

——, and P. Klein, 2006: Dynamics of the upper oceanics layers in terms of surface quasigeostrophy theory. *J. Phys. Oceanogr.,* **36,** 165–176.

Le Traon, P. Y., P. Klein, B. L. Hua, and G. Dibarboure, 2008: Do altimeter wavenumber spectra agree with the interior or surface quasigeostrophic theory? *J. Phys. Oceanogr.,* **38,** 1137–1142.

Lindzen, R. S., 1994: The Eady problem for a basic state with zero PV gradient but $\beta \neq 0$. *J. Atmos. Sci.,* **51,** 3221–3226.

Longuet-Higgins, M. S., 1968: The eigenfunctions of Laplace's tidal equations over a sphere. *Philos. Trans. Roy. Soc. London,* **262A,** 511–607, doi:10.1098/rsta.1968.0003.

Pedlosky, J., 1987: *Geophysical Fluid Dynamics*. 2nd ed. Springer-Verlag, 710 pp.

Philander, S. G. H., 1978: Forced oceanic waves. *Rev. Geophys.,* **16,** 15–46.

Samelson, R. M., 1992: Surface-intensified Rossby waves over rough topography. *J. Mar. Res.,* **50,** 367–384.

Tulloch, R., and K. S. Smith, 2006: A theory for the atmospheric energy spectrum: Depth-limited temperature anomalies at the tropopause. *Proc. Natl. Acad. Sci. USA,* **51,** 2756–2768.

——, and ——, 2009: Quasigeostrophic turbulence with explicit surface dynamics: Application to the atmospheric energy spectrum. *J. Atmos. Sci.,* **66,** 450–467.

Wang, D.-P., C. N. Flagg, K. Donohue, and H. T. Rossby, 2010: Wavenumber spectrum in the Gulf Stream from shipboard ADCP observations and comparison with altimetry measurements. *J. Phys. Oceanogr.,* **40,** 840–844.

Wunsch, C., 1997: The vertical partition of oceanic horizontal kinetic energy. *J. Phys. Oceanogr.,* **27,** 1770–1794.

——, and D. Stammer, 1997: Atmospheric loading and the oceanic ''inverted barometer'' effect. *Rev. Geophys.,* **35,** 79–107.